Zhang *et al. Biochar* (2024) 6:30
https://doi.org/10.1007/s42773-024-00317-2

Biochar

ORIGINAL RESEARCH

Open Access

Roles of biochars' properties in their water-holding capacity and bound water evaporation: quantitative importance and controlling mechanism

Huiying Zhang[1], Yue Cheng[1], Yinhua Zhong[1], Jinzhi Ni[1], Ran Wei[1] and Weifeng Chen[1*]

Abstract

Important properties of biochar as an effective soil amendment are its high water-holding capacity (WHC) and inhibition of water evaporation. However, the mechanism and the importance of biochar properties in controlling its own WHC and bound water evaporation remain little known. In this study, wheat straw and pine sawdust biochars were pyrolyzed in N_2-flow, CO_2-flow, and air-limitation environments at 300–750 ℃, and a series of the produced biochars' properties were characterized to explore the dominant controlling factors of their WHC and bound water evaporation. The results have shown that with the increasing contents of hydrogen, nitrogen, and oxygen as well as such ratios as H/C, and (O + N)/C, WHC of the biochars was also increasing while the evaporation of biochar-bound water was decreasing. With an increase in the other studied factors, such as carbon content, pH, and specific surface area (SSA), WHC of the biochars was decreasing, and the evaporation of biochar-bound water was increasing. That was connected with the fact that biochar-nitrogen was mainly in pyridinic and pyrrolic forms, while oxygen was in the form of C = O and C–O bonds. These forms of nitrogen and oxygen could be the receptors of hydrogen bonds to link to H_2O molecules. Aliphatic hydrogen with a weak positive charge could be a donor of hydrogen bonds to link to H_2O molecules. However, high carbon content, as well as high SSA, indicated more exposed aromatic carbon (hydrophobic sites) that could suppress the binding of H_2O molecules. Additionally, high pH indicated that H_2O molecules were dominated by OH^-, which generated strong electrostatic repulsion with the negatively charged nitrogen- and oxygen-containing groups of biochar. It was also shown that the nitrogen-containing groups played a more important role (importance – 0.31) in WHC of the biochar than other parameters, including carbon, oxygen, hydrogen, ash contents, pH, SSA (importance from 0.02 to 0.09). Nitrogen, oxygen, and carbon contents had the most important influence on the evaporation of biochar-bound water in all studied factors. Furthermore, wheat straw biochar produced at low pyrolysis temperatures in N_2 atmosphere (with high nitrogen and oxygen contents) had the highest WHC and the lowest evaporation of biochar-bound water. Consequently, it can be suggested that biochar rich in nitrogen can be an effective water retention agent and can improve agricultural soil moisture.

Handling editor: Hailong Wang

*Correspondence:
Weifeng Chen
CWF_geo@fjnu.edu.cn; fengweichen1986@163.com
Full list of author information is available at the end of the article

Highlights

- Nitrogen-containing groups (pyridinic and pyrrolic nitrogen) played a crucial role in the improvement of biochar water-holding capacity.
- Nitrogen- and oxygen-containing groups inhibited the evaporation of biochar-bound water.
- Biochar rich in nitrogen and oxygen may be an effective water retention agent to maintain soil moisture.

Keywords Biochar, Properties, Water-holding capacity, Evaporation of biochar-bound water, Hierarchical partitioning

Graphical Abstract

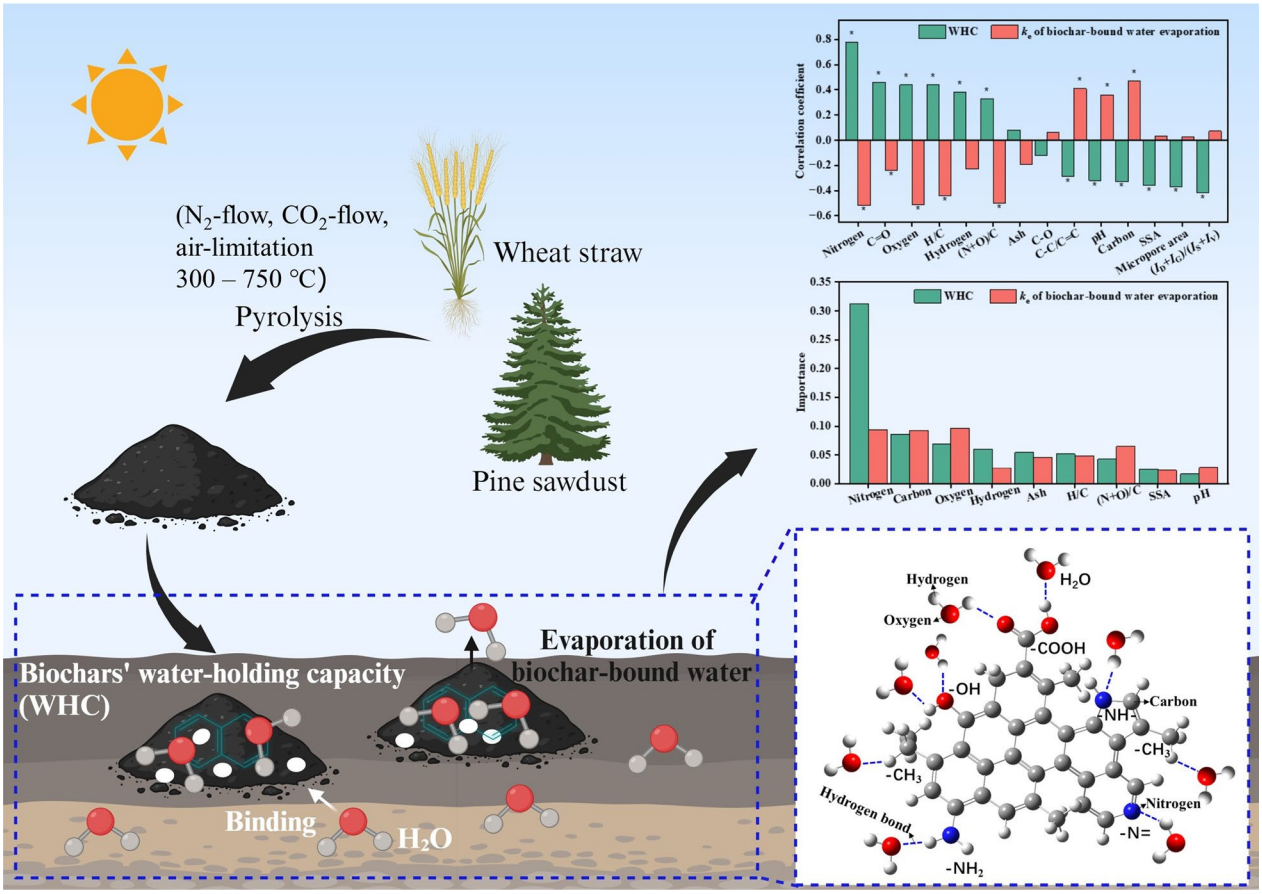

1 Introduction

Biochar is a high temperature-pyrolytic biomass-derived carbon-rich material produced in an anoxic environment, and it has a variety of outstanding features (e.g., wide source of raw materials, high specific surface area (SSA), developed porosity, rich functional groups, and high content of stable carbon), thus its application to soils has attracted widespread attention (Weber and Quicker 2018; Xiang et al. 2022; Jang and Kan 2019). The existing research mainly focuses on the applications of biochar for pollutant adsorption, carbon sequestration, and agricultural soil improvement (Wu et al. 2022; Hamidzadeh et al. 2023; Gao et al. 2022; Liu et al. 2021). The significance of biochar in agriculture was attributed to the improvement in soil water-holding capacity (WHC) (Adhikari et al. 2022; Lataf et al. 2022; Zhang et al. 2020). Drought and water stress reduce soil fertility, thus lowering the crop yield. Biochar has been found to improve soil WHC and combat water stress owing to its excellent properties (e.g., porosity, SSA, and polar groups) and its

interactions with soil particles (Werdin et al. 2021; Ibrahimi and Alghamdi 2022).

Biochar-related improvement in soil WHC partially results from the modified soil properties induced by the interactions between soil particles and biochar (Omondi et al. 2016; Blanco-Canqui 2017; Mao et al. 2019). On one hand, biochar interaction with soil particles can result in the formation of macroaggregates with higher SSA and porosity, eventually providing more binding sites for water molecules and increasing the WHC of soil (Adhikari et al. 2022; Yang et al. 2021; Zhang et al. 2021; Seitz et al. 2020). On the other hand, soil with high macropore content is characterized by faster water movement and lower WHC, and biochar (small particle size) application to such soil can reduce the macropore volume, increase the available WHC, and reduce water movement (Zhang et al. 2016; Basso et al. 2013).

Except for altering the properties of soil, the WHC of biochar-amended soil is largely controlled by the WHC of biochar-self (Mao et al. 2019; Adhikari et al. 2023). It has been reported that biochar with low hydrophilicity (high WHC) could improve soil hydrophilicity thus affecting the WHC of soil, and vice versa (Mao et al. 2019). Hence, it is necessary to investigate the WHC of biochar-self and its controlling factors (Adhikari et al. 2023; Lataf et al. 2022). The existing works suggest that the WHC of biochar can vary from 52 wt.% to 924 wt.%, and wide WHC range is attributed to biochar's diverse properties (Lataf et al. 2022; Adhikari et al. 2023). For example, increasing specific surface area (SSA) and porosity of biochar can improve its WHC by exposing more hydrophilic sites and improving pore-filling effects (Lataf et al. 2022; Gray et al. 2014; Adhikari et al. 2022 and 2023; Zornoza et al. 2016). Besides, the WHC of biochar is strongly related to its sphericity, surface functionality, and particle size (Adhikari et al. 2023; Wiersma et al. 2020). Biochar with a smooth surface presents a low WHC (Oppong Danso et al. 2021; Zornoza et al. 2016; Mao et al. 2019). Functional group analysis indicates that biochar with high WHC lacks the aliphatic CH_2 and aromatic C=C (Mao et al. 2019; Adhikari et al. 2022, 2023). Suliman et al. (2017) reported that the surface oxygen-containing groups (e.g. carboxylic groups) of biochar could increase its WHC by improving the hydrophilicity of biochar. Accordingly, it can be concluded that the WHC of biochar is co-controlled by multi-properties of biochar including the chemical compositions (elemental compositions, and chemical groups), carbon structure (graphitic structure and aliphatic structure), pore volume and SSA (Adhikari et al. 2022, 2023; Mao et al. 2019; Zornoza et al. 2016). However, the quantitative contributions of the various properties of biochar to their WHC remains unknown, which hinders the understanding of the dominant mechanism controlling the WHC of biochar and the regulation of biochar producing conditions to improve its WHC. Furthermore, the intensification of global warming can accelerate the evaporation of soil moisture. The evaporation of biochar-bound water can directly reflect the affinity of biochar to water molecules. Exploring and quantifying the main controlling factors of biochar-bound water evaporation is helpful for the production of biochar suitable for soil modification in terms of soil water stress caused by global warming.

Pyrolysis temperature and atmosphere are two main regulatable factors controlling the properties of biochar and its WHC (Li and Tan 2021; Mao et al. 2019). For example, Li and Tan (2021) found that rice straw biochar produced at 400 – 800 ℃ in N_2 or CO_2 atmosphere had the WHC ranging from 562.3 to 835.05 wt%; wherein, biochar produced at 400 °C and 800 ℃ had a greater WHC than that of biochar produced at 600 ℃. They have also found that the 400 ℃ biochar had more polar groups (mainly –OH and –COOH) and the 800 ℃ biochar had more porosity than the 600 ℃ biochar. At the same time, the WHC of biochar produced in CO_2 was greater than that produced in N_2, because biochar produced in CO_2 contained more polar groups and had higher porosity than that produced in N_2. Except for N_2 and CO_2, air-limitation is another pyrolytic atmosphere to produce biochar, and biochar produced in air-limitation atmosphere had different properties (e.g., elemental compositions, porosity, functional groups, and aromaticity) from the biochars produced in N_2 and CO_2 atmospheres (Wu et al. 2022; Yu et al. 2022). Therefore, a series of biochars with different properties were produced under different pyrolytic temperatures and atmospheres in this study. Quantify the importance of different properties on the WHC of biochar and the evaporation of biochar-bound water. Therefore, in this study, a series of biochars with different properties were produced under different pyrolytic temperatures and atmospheres to explore the mechanism and quantify the importance of different properties on the WHC of biochar and the evaporation of biochar-bound water. The results of the study are greatly significant for the directional design of biochar for its practical application to increase the WHC of agricultural soils and to reduce the water stress of crops.

2 Materials and methods

2.1 Pyrolysis of biomass into biochar

In this work, two feedstocks including wheat straw and pine sawdust were charred in three types of atmospheres (N_2-flow, CO_2-flow, and air-limitation) and at four pyrolytic temperatures (300, 450, 600, and 750 ℃) to produce different biochars. To produce biochar in N_2- and CO_2-flows, about 110 g of the given feedstock was

charred in a tube furnace (O-KTF1200, Jiangsu, China) at the set temperature (300, 450, 600, and 750 ℃) for 5 h, and the heating rate of 20 ℃ min^{-1}. High-purity N_2/CO_2 was blown through the tube furnace at the flow rate of 0.5 L min^{-1}. To produce biochar in air-limitation atmosphere, the feedstocks were charred in the tube furnace without any gas flow (only the initial air, about 8 L at normal temperature and pressure, remained in the tube). Afterward, the obtained products (biochars) were cooled down to below 50 ℃, taken out, milled, and passed through a sieve with 0.15 mm aperture, then stored in a dryer.

2.2 Biochar characteristics

The content of ash (wt.%) was measured by placing the sample in a quartz boat in a muffle furnace and heated at 750 ℃ for four hours (Chen et al. 2019). The contents (wt.%) of three main elements including carbon, hydrogen, and nitrogen were quantified using an elemental analyzer (Vario ELIII, Thermo Fisher Technology (China) Co., LTD). The oxygen content was determined as the remainder, based on the assumption that the sum of the five components (ash, carbon, nitrogen, hydrogen, and oxygen) was 100% (Nzediegwu et al. 2021; Wang et al. 2013). All the measurements were done in triplicates for each studied biochar sample.

FTIR spectrometer (Nexus 460) with a wavenumber range of 400–4000 cm^{-1} was applied to identify the functional groups on the biochars (Additional file 1: Fig. S1). A Raman system (Renishaw inVia 2000) was applied to quantify the graphitization of the biochars. The Raman system setting was: the excitation wavelength – 785 nm; the spectral wavenumber range – 500 – 2750 cm^{-1}; the wavenumber resolution – 3 – 5 cm^{-1}. In Origin 2023a software, the spectrum peak at 800–2000 cm^{-1} was divided into four subpeaks (S – 1185 cm^{-1}, D – 1345 cm^{-1}, V – 1460 cm^{-1}, and G – 1590 cm^{-1} bands) by Gaussian model and deconvolution algorithm. The intensities of S, D, V, and G bands were characterized by the bands' areas and expressed as I_S, I_D, I_V, and I_G, respectively. The ratio $(I_D+I_G)/(I_S+I_V)$ indicates the graphitization of biochars: the greater the value, the stronger graphitization (Chen et al. 2021; Kim et al. 2011).

The main surface elements and oxygen/nitrogen-containing functional groups of the biochars were analyzed using XPS (ThermoScientifc K-Alpha). Using the Gaussian model in Origin 2023a the C1s peak (the signal peaks of 1 s electron energy levels of carbon atoms) in XPS was divided into three subpeaks (Li et al. 2020; Singh et al. 2014): at 284.8 eV (C–C/C=C group), at 286.3 eV (C–O group), and at 287.5 eV (C=O group); while the obtained N1s peak (the signal peaks of 1 s electron energy levels of nitrogen atoms) was also divided into three subpeaks (Yang et al. 2023; Lazar et al. 2019): at 398.5 eV (pyridinic nitrogen), at 399.4 eV (amine-nitrogen), and at 400.2 eV (pyrrolic nitrogen). The carbon contents of the carbon-containing groups (wt.%) in biochars are equal to the abundance of carbon-containing groups × carbon content (wt.%). The results are shown in Additional file 1: Table S1.

The pore volume and SSA of the biochars were measured by the adsorption–desorption isotherm of high purity N_2 at a liquid nitrogen temperature (77 K) in a Micro ASAP2460 surface area analyzer. The biochar samples (0.3 g) were degassed in a vacuum at 473 K for 12 h (Muzyka et al. 2023). The density functional theory (DFT) model was used to analyze the micropore area (with a diameter less than 2 nm) and SSA of the biochars (Leng et al. 2021).

2.3 Biochar WHC and bound water evaporation

The WHC of the biochars was measured using a modified determination method (Lataf et al. 2022) in three replicates. Briefly, 0.50 g of biochar was mixed with 20 mL of deionized water in a 20 mL glass vial, and the vial was shaken at 25 ℃ (100 r min^{-1}) for 3 days. After that, when the biochar was fully saturated, the biochar/water mixture was passed through a quantitative filter paper (diameter – 112.5 cm, maximum aperture – 15–20 μm) in a funnel until the water stopped dripping down. The water-saturated biochar samples with filters were dried at 105 ℃ for 12 h and weighed. Along with the biochar samples, blank filter paper was put through the same procedure to calculate the amount of water absorbed by the filter. The WHC of biochar was calculated using Eq. (1):

$$\mathrm{WHC} = \left(m_{sb} - m_{fp} - m_{bc}\right)/m_{bc} \quad (1)$$

where m_{sb} (*g*), m_{fp} (*g*), and m_{bc} (*g*) were the masses of the water-saturated biochar with filter paper, the water-saturated filter paper, and the dry biochar, respectively.

To measure evaporation of biochar-bound water, the method similar to WHC measurement was used: after the biochar samples were saturated with water, they were dried in an oven at 40 ℃ (40 ℃ is a common temperature in scorching weather) and weighed every 15 min until the sample weight reached an equilibrium. The evaporation of biochar-bound water is equal to the water retention without filter paper at each time (WR_t) divided by WHC (Fig. 1). The evaporation kinetics of biochar-bound water are calculated using first-order kinetic equation:

$$\mathrm{WR}_t/\mathrm{WHC} = \exp\left(-k_e \times t\right) \quad (2)$$

where, *t* (min) is the weighing time, WR_t (g g^{-1}) is the water retention without filter paper at the time *t*, k_e (min^{-1}) is the first-order kinetic constant. In this study,

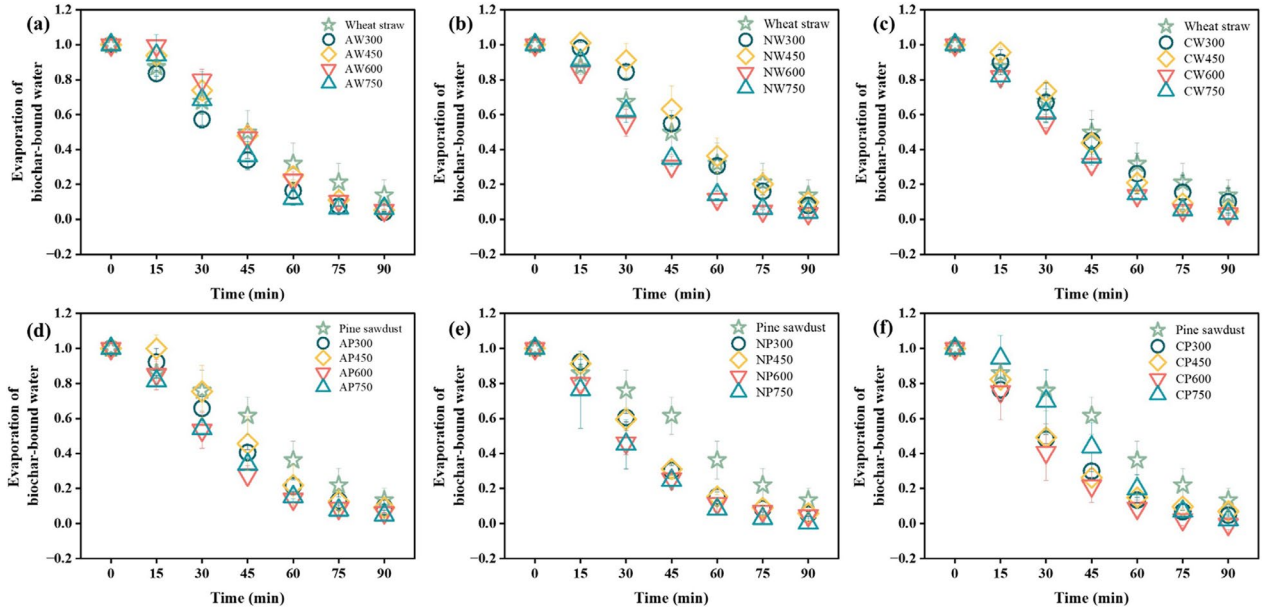

Fig. 1 Evaporation kinetics of biochar-bound water. Biochars: **a** AW – wheat straw biochar produced in air-limitation, **b** NW – wheat straw biochar produced in N_2-flow, **c** CW – wheat straw biochar produced in CO_2-flow, **d** AP – pine sawdust biochars produced in air-limitation, **e** NP – pine sawdust biochars produced in N_2-flow, and **f** CP – pine sawdust biochars produced in CO_2-flow. The numbers 300, 450, 600, and 750 represent the pyrolytic temperature

the fitting coefficient (R^2) > 0.85 for the first-order kinetic equation indicated that the biochar-bound water evaporation data was suitable for the first-order kinetic equation.

2.4 Statistical analysis and molecular simulation

To testify the effects of the studied properties of the biochars on the biochar's WHC and evaporation of biochar-bound water, the correlation analysis between the properties of the biochars and the WHC or first-order kinetic constant, k_e (min^{-1}) of the evaporation of biochar-bound water was conducted. The hierarchical partitioning method was used to analyze the importance of the biochar properties in controlling the WHC and water evaporation. The R package "*rdacca.hp*" introduces the concept of hierarchical partitioning to assign individual effects to each explanatory variable under all possible model subsets, providing a new quantitative index for evaluating the relative importance of linear explanatory variables in the hierarchical partitioning (Lai et al. 2022). In addition, it has become an important tool for importance quantification of factors. In this experiment, this R software package was used to study the relative importance of the studied biochar properties to WHC and k_e values with the properties of biochar as explanatory variables and WHC and k_e values as response variables (Lai et al. 2022).

To clarify the controlling mechanism, the electrostatic potential charge of the main biochar functional groups was calculated by molecular simulation. Part of the molecular structure of biochar was drawn by ChemOffice 2004. The charges of different atoms (e.g., alkyl carbon, pyridinic nitrogen, amine-nitrogen, pyrrolic nitrogen, hydroxyl oxygen, and carbonyl oxygen) on biochar were simulated and calculated in DFT (B3LYP) method using GaussView 5.0. The electrostatic potential charge of atoms in different biochar chemical groups is shown in Table 1.

The variability of different biochar properties was calculated using the equation: variability = standard deviation/average value. Greater temperature variability value indicated a greater influence of pyrolysis temperature on the studied properties of the biochars (Zhao et al. 2013). The correlation between the properties of the biochars, with their WHC and evaporation of water was analyzed by Origin2023a. SPSS 25.0 software was used to analyze the significance of differences. The equation fitting of the data was carried out using Sigmaplot 12.5. The plot was performed in Origin 2023a software.

3 Results and discussion

3.1 Biochar properties

The studied biochar (24 types) properties (main chemical compositions, functional groups, pH, polarity, graphitization, and SSA) are summarized in Fig. 2

Table 1 Electrostatic potential charges of atoms in different chemical groups on biochar

Groups	Carbon charge	Hydrogen charge	Nitrogen charge	Oxygen charge
H_2O	–	0.326	–	–0.653
$-CH_2-$, $-CH_3$	– 0.467–– 0.620	0.171–0.223	–	–
$C-NH_2$	0.334	0.308–0.311	– 0.835	–
–C=N–C=	0.068–0.079	–	– 0.552	–
=C–NH–C=	0.081–0.367	0.337	– 0.823	–
C=O	0.655	0.365	–	– 0.505
C–OH	0.261–0.655	0.365–0.372	–	– 0.593–– 0.618

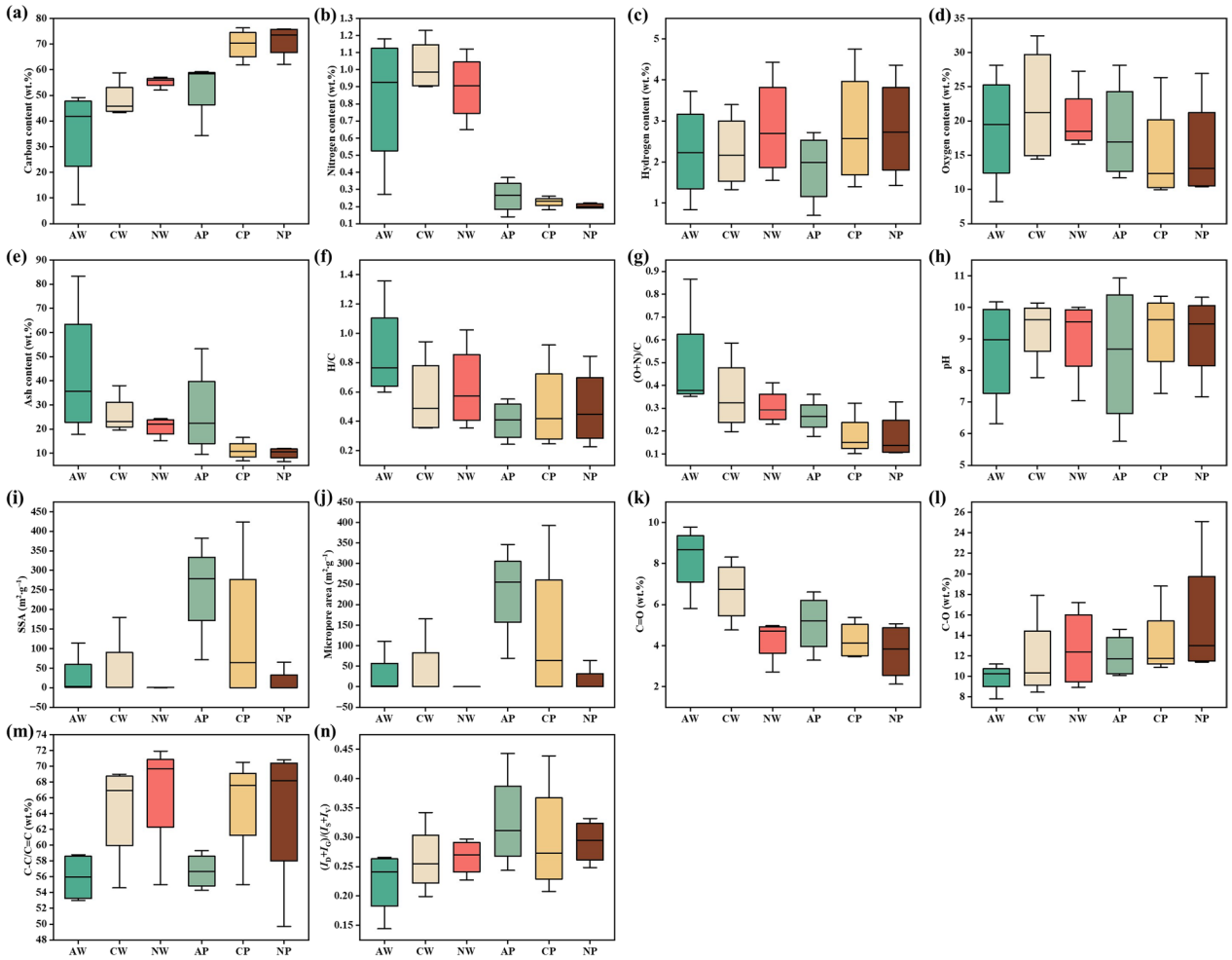

Fig. 2 The properties of biochars. Biochars: AW – wheat straw biochar produced in air-limitation, CW – wheat straw biochar produced in CO_2-flow, NW – wheat straw biochar produced in N_2-flow, AP – pine sawdust biochars produced in air-limitation, CP – pine sawdust biochars produced in CO_2-flow, and NP – pine sawdust biochars produced in N_2-flow. SSA – specific surface area

and Additional file 1: Table S1. The content of hydrogen in the studied biochar samples was changed from 0.70 ± 0.00 to 4.75 ± 0.02 wt.%, of carbon—from 7.39 ± 0.02 to 76.31 ± 0.02 wt.%, of nitrogen—from 0.14 ± 0.01 to 1.23 ± 0.03 wt.%, of oxygen—from 8.22 ± 0.29 to 32.45 ± 0.32 wt.% and of ash—from 6.49 ± 0.05 to 83.27 ± 0.25 wt.%. The variability of these parameters was 0.45, 0.28, 0.69, 0.39, and 0.75, respectively (Fig. 2a–e, Fig. 3). The ratios H/C and (O + N)/C are respectively used to indicate aliphiticity and polarity

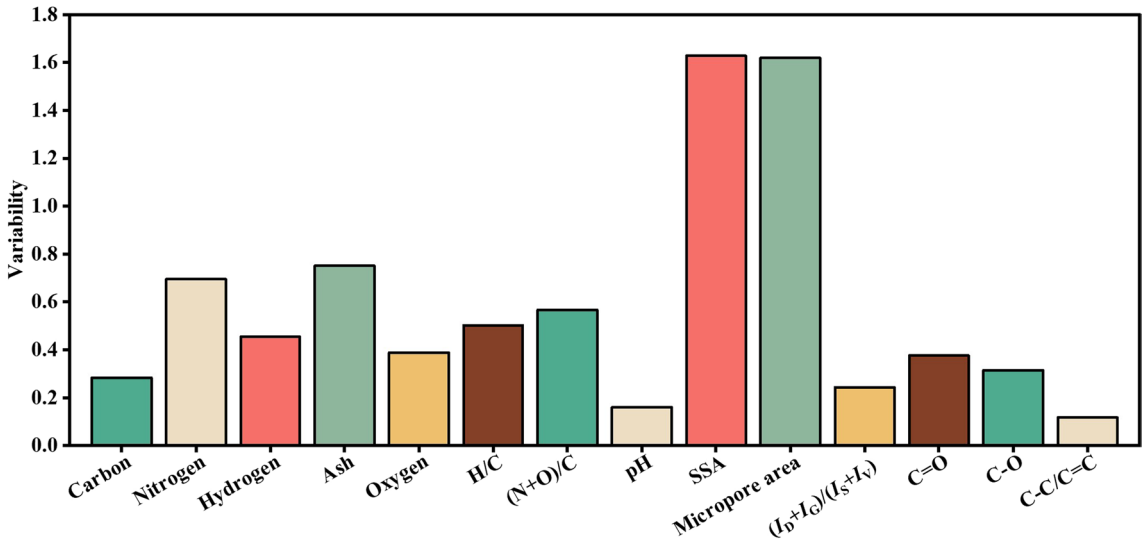

Fig. 3 The variability of the biochars' properties. SSA – specific surface area

of biochar. The ratios increase with increasing aliphaticity or polarity. For the studied biochars, the H/C ratio ranged from 0.23 to 1.36, while (O + N)/C ratio ranged from 0.1 to 0.87, and their variability was 0.50 and 0.57, respectively (Fig. 2f, g, Fig. 3). The pH of the studied biochars ranged from 5.05 ± 0.07 to 10.93 ± 0.01 (with variability of 0.16). The SSA of the biochars changed from 0.16 to 423.78 $m^2\ g^{-1}$ while micropore area – from 0 to 392.62 $m^2\ g^{-1}$, and their variability was 1.63 and 1.62 (Fig. 2i, j, Fig. 3), respectively. In the FTIR spectrum (Additional file 1: Fig. S1), the signals of some typical functional groups (e.g., -COOH, and -OH) could be found for the biochars produced at the low pyrolytic temperatures (300 – 450 ℃), while they were not present in the biochars of the high pyrolytic temperatures (600 – 750 ℃), with an exception of wheat straw biochar from air-limitation pyrolysis where the composition of the functional groups did not change with an increase in the pyrolytic temperature. The semi-quantification of C = C/C–C, C–O, and C = O groups based on the XPS analysis indicated that the carbon content of C = C/C–C, C–O, and C = O groups was from 32.0 to 71.9, from 7.81 to 24.2, and from 2.13 to 9.78, respectively, with variability of 0.11, 0.31, and 0.38, respectively (Fig. 2k–m, Fig. 3). Based on the publications, S (1185 cm^{-1}) and V (1460 cm^{-1}) bands indicate aliphatic/amorphous carbon, while D (1345 cm^{-1}) and G (1590 cm^{-1}) bands indicate aromatic/graphitic carbon (Chen et al. 2014; Kim et al. 2011). The $(I_D + I_G)/(I_S + I_V)$ ratio, which increases with the increasing aromaticity, can be applied to characterize the aromaticity of biochars. For the studied biochars, this ratio changed from 0.14 to 0.44 with a variability of 0.24 (Fig. 2n, Fig. 3).

In conclusion, the variability for most of the measured properties of the biochars was moderate – greater than 0.25, suggesting that the properties are related to the biochar production conditions, thus can be used to quantify the importance of the studied properties of the biochars for their WHC and the evaporation of biochar-bound water (Zhao et al. 2013).

3.2 The mechanism and importance of various biochar properties to its WHC

Of all the studied biochars, wheat straw biochar produced in N_2-flow at 300 ℃ (WHC – 8.0 g g^{-1}) was characterized by the highest WHC, while the pine sawdust biochar produced in CO_2-flow at 600 ℃ (WHC – 1.8 g g^{-1}) by the lowest WHC (Fig. 4a, b). Under the same conditions (pyrolytic temperature and atmosphere), the pine sawdust biochar always exhibited lower WHC values than wheat straw biochar. This result was consistent with the results of Wiersma et al. (2020). The WHC values of the wheat straw biochars and the pine sawdust biochar N_2-flow generally declined with the elevating pyrolytic temperature, which was related to the decreasing (O + N)/C ratio (hydrophilic site) and increasing aromaticity (hydrophobic site) of the biochars (Additional file 1: Table S1) (Suliman et al. 2017; Hien et al. 2021). Meanwhile, at 300–450 ℃, biochar produced in N_2-flow and air-limitation exhibited greater WHC values than that produced in CO_2-flow except the pine sawdust biochar produced at 450 ℃. This may be due to the higher H/C value (aliphaticity) of this type of biochar (Additional file 1: Table S1), which can provide more weak hydrogen bond sites (Hien et al. 2021; Gilli and Gilli 2014). At 600–750 ℃, biochars produced in air-limitation

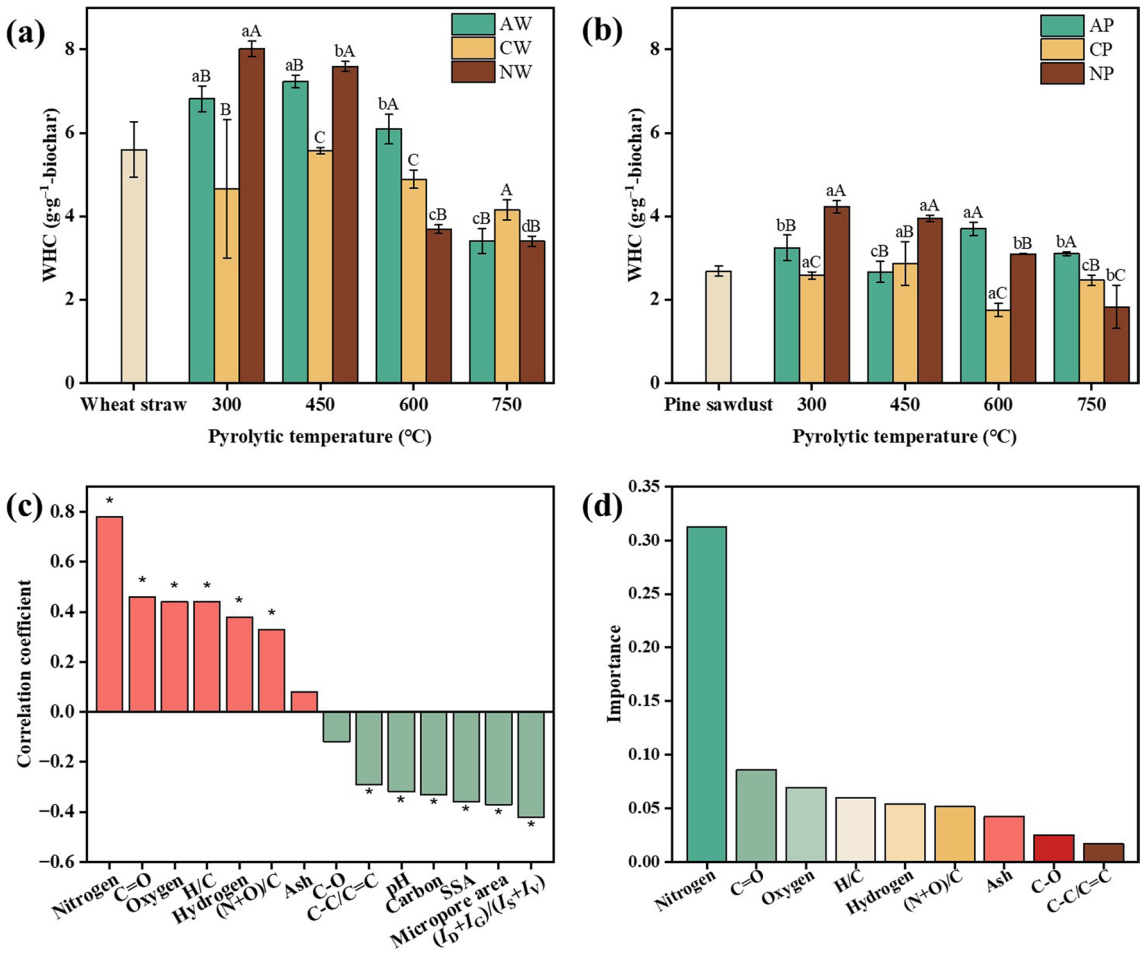

Fig. 4 **a**, **b** The WHC of biochars, **c** Correlation between the properties and the WHC of biochars, **d** The importance of properties to the WHC of biochars. Biochars: AW – wheat straw biochar produced in air-limitation, CW – wheat straw biochar produced in CO_2-flow, NW – wheat straw biochar produced in N_2-flow, AP – pine sawdust biochars produced in air-limitation, CP – pine sawdust biochars produced in CO_2-flow, and NP – pine sawdust biochars produced in N_2-flow. Different lowercase letters indicate the significant differences in the spectral index among different pyrolysis temperatures, and different uppercase letters indicate the significant difference in the spectral index among different pyrolysis atmospheres (Tukey test, $p < 0.05$). "*" indicates a significant correlation. SSA – specific surface area

had the maximum WHC values, but wheat straw biochars produced in CO_2-flow at 750 ℃ presented the highest WHC.

The correlation analysis was further used to evaluate the roles of various studied biochar properties on the biochars' WHC. The results are shown in Fig. 4c. The WHC of the biochars showed a significant negative correlation ($p < 0.05$) with the biochar carbon content, pH, SSA, and micropore area, and a significant positive correlation ($p < 0.05$) with hydrogen, nitrogen, and oxygen contents, H/C ratio, and (O + N)/C ratio. High carbon content combined with low H/C and (O + N)/C indicates high aromaticity, low polarity, and high hydrophobicity of biochar surface, resulting in the lower WHC of biochar (Mao et al. 2019; Adhikari et al. 2023). According to the data in Additional file 1: Table S1, the biochars produced at high pyrolytic temperatures (600–750 ℃) were characterized by high SSA and micropore area. When produced at these high temperatures, the biochars had low values of H/C and (O + N)/C ratios (high aromaticity and low polarity), thus high SSA and micropore area exposed more aromatic carbon and hydrophobic sites and that finally resulted in lower WHC of the biochars. Higher hydrogen content and H/C value indicate more aliphatic carbon (e.g., alkylate carbon). According to the molecular simulation, the hydrogen of the aliphatic structure with weakly positive charge (hydrogen charge is about − 0.171–0.223) could be a donor of hydrogen bond to link to the H_2O molecule (oxygen of H_2O with the charge of − 0.653 can be the receptor of hydrogen bond) (Table 1 and Fig. 5e) (Gilli and Gilli 2014). Hence, hydrogen content and H/C value presented a significantly positive

correlation with the WHC of biochar. High nitrogen, and oxygen content, as well as values of (O + N)/C ratio characterize biochars with higher content of polar functional groups (Suliman et al. 2017; Adhikari et al. 2022, 2023). According to the XPS analysis, the biochar nitrogen was mainly in pyridinic and pyrrolic forms, while oxygen was in the form of C = O and C–O bonds (Fig. 5, Additional file 1: Fig. S2 and S3). These forms of nitrogen and oxygen have strong negative charge (nitrogen charge from − 0.552 to − 0.835, oxygen charge from − 0.505 to − 0.618) (Table 1) and unshared electronic pairs, which could be a receptor of hydrogen bond to link to H_2O molecule (hydrogen of H_2O with charge of 0.326 can be the donor of hydrogen bond) (Gilli and Gilli 2014) (Fig. 5e). Therefore, nitrogen content, oxygen content, and (O + N)/C values all had significantly positive correlations with the WHC of the biochars. The biochars' pH values had a negative correlation with the biochars' WHC (Fig. 4c) presumably because high pH transformed most of the H_2O molecules into the form of OH^- which generates strong electrostatic repulsion of the negatively charged nitrogen- and oxygen-containing groups of the biochars.

The hierarchical partitioning method was adopted to quantify the importance of the studied properties of the biochars to its WHC. Interestingly, though nitrogen content was the lowest (from 0.18 ± 0.03 to 1.23 ± 0.03 wt.%; Fig. 2b) in the element compositions of biochars, it played the most important role (importance – 0.31) in the WHC of the biochars than the other studied parameters, including carbon, oxygen, hydrogen, and ash content, pH, and SSA, which had relatively similar importance (0.02–0.09). On one hand, H_2O can be attached to the surface of biochar mainly via the hydrogen bond. Nitrogen in the biochars was mainly in the form of pyridinic and pyrrolic nitrogen (nitrogen charge—from − 0.823 to − 0.552) (Fig. 5 and Additional file 1: Fig. S3) which had a greater ability to form hydrogen bonds than aliphatic hydrogen (hydrogen charge—from 0.171 to 0.223) and oxygen (C = O and C–O) (oxygen charge—− 0.505), bind more easily to H_2O molecules (hydrogen charge—0.326, oxygen charge—− 0.653) (Gilli and Gilli 2014). On the other hand, nitrogen content had high variability (0.69) compared to the other studied properties (carbon—0.28; hydrogen—0.45; oxygen—0.39) with varied pyrolytic conditions (Fig. 3). Thus nitrogen content could make a more significant change in WHC of the biochars than the other studied properties. Though ash content and SSA had higher variability (0.75 and 1.63, respectively) than nitrogen content (0.69), their importance in affecting the WHC of the biochar was lower than that of nitrogen content. That was because ash had no significant correlation with the WHC of biochar, and SSA is not conducive to increasing the WHC of biochar. Above all, nitrogen-containing groups were the most important factor in affecting the WHC of biochar, thus increasing the nitrogen content in biochar could be an effective way to improve its WHC.

3.3 The mechanism and importance of various biochar properties in controlling the evaporation of biochar-bound water

As shown in Fig. 6a, b, wheat straw biochar-bound water had lower k_e (from 0.0167 ± 0.0026 to 0.0261 ± 0.0029 min^{-1}) than pine sawdust biochar-bound water (from 0.0193 ± 0.0024 to 0.0326 ± 0.0030 min^{-1}) under the same pyrolytic conditions. Oxygen- and nitrogen-containing functional groups form strong hydrogen bonds with H_2O and possibly it is the most important factor in reducing the evaporation of biochar-bound water. However, oxygen content in the wheat straw biochar was from 8.22 ± 0.29 to 32.45 ± 0.32 wt.% (mean 22.19 wt.%) and did not differ much from its content in pine sawdust biochar from 9.98 ± 0.11 to 28.15 ± 0.21 wt.% (mean 18.51 wt.%). Therefore, lower k_e of wheat straw biochar-bound water must have been related to the higher content of nitrogen-containing functional groups of which it was from 0.27 ± 0.02 to 1.23 ± 0.03 wt.%, (mean–0.92 wt.%) in wheat straw biochar and from 0.19 ± 0.04 to 0.37 ± 0.02 wt.% (mean–0.22 wt.%) in pine sawdust biochar. The negatively charged nitrogen-containing groups (mainly the pyridinic and pyrrolic nitrogen, Fig. 5) could be important hydrogen bond receptor to reduce the evaporation of biochar-bound water. Furthermore, the evaporation of biochar-bound water generally increased with the elevating pyrolytic temperatures. For instance, in the pyrolytic atmosphere of N_2-flow, wheat straw biochar produced at 300–450 °C had lower k_e (from 0.0167 ± 0.0026 to 0.0180 ± 0.0025 min^{-1}) than that produced at 600–750 °C (from 0.0237 ± 0.0023 to 0.0261 ± 0.0029 min^{-1}); likewise, pine sawdust biochar produced at 300–450 ℃ had lower k_e (from 0.0240 ± 0.0027 to 0.0240 ± 0.0026 min^{-1}) than that produced at 600–750 ℃ (k_e from 0.0283 ± 0.0024 to 0.0308 ± 0.0029 min^{-1}). The primary reason for that must have been the fact that with the elevating temperature, the nitrogen and oxygen contents in biochars were decreasing, while the carbon content (hydrophobic structure) was increasing. An exception was the wheat straw biochar produced in air-limitation, which exhibited higher k_e at 300 ℃ (0.0250 ± 0.0021 min^{-1}) than at 450 – 750 ℃ (from 0.0197 ± 0.0031 to 0.0225 ± 0.0037 min^{-1}), though the former had the highest nitrogen and oxygen contents in all the wheat straw biochars produced in air-limitation. Wheat straw biochar produced at 300 ℃ in air-limitation also presented the highest H/C content (aliphatic hydrogen). Aliphatic hydrogen could form weaker

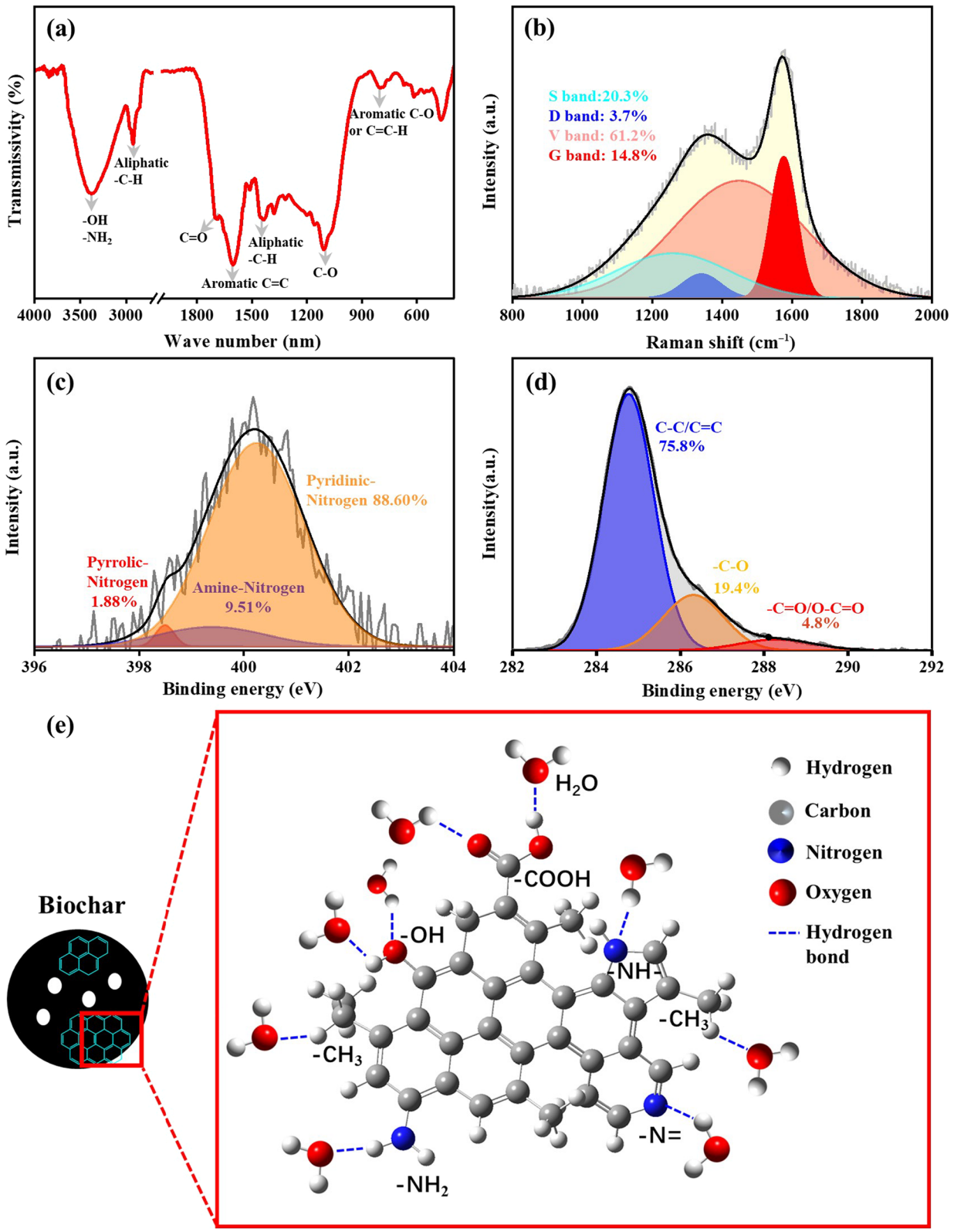

Fig. 5 For wheat straw biochar produced in N_2-flow at 300 ℃: **a** Fourier transform infrared (FTIR) spectra of biochar; **b** Raman spectra of biochar; **c** N1s peak in X-ray photoelectron spectroscopy (XPS) spectra of biochar; **d** C1s peak in X-ray photoelectron spectroscopy (XPS) spectra of biochar; **e** Molecular structure simulation of biochar

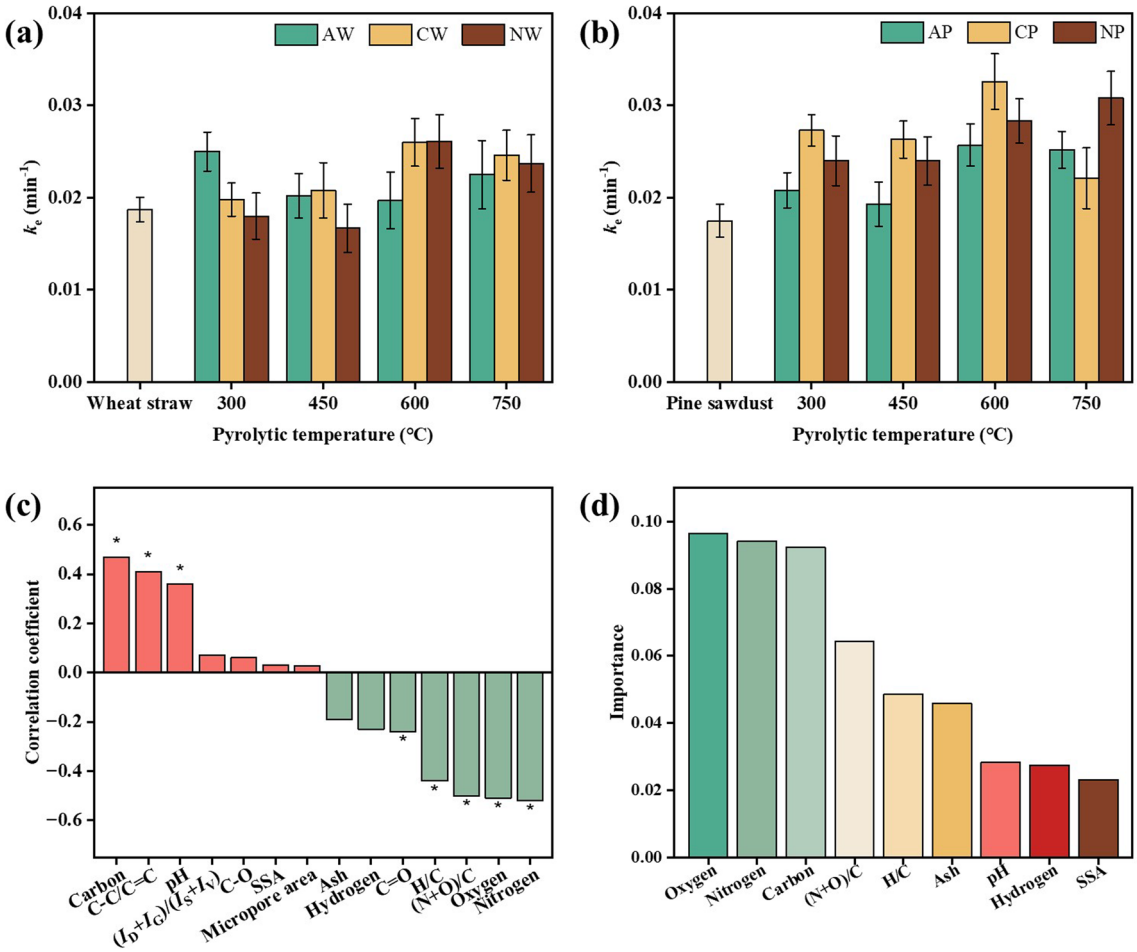

Fig. 6 **a**, **b** The evaporation kinetic constant (k_e) of biochar-bound water, **c** Correlation between the properties and k_e of biochar-bound water, and **d** The importance of properties to k_e of biochar-bound water. Biochars: AW – wheat straw biochar produced in air-limitation, CW – wheat straw biochar produced in CO_2-flow, NW – wheat straw biochar produced in N_2-flow, AP – pine sawdust biochars produced in air-limitation, CP – pine sawdust biochars produced in CO_2-flow, and NP – pine sawdust biochars produced in N_2-flow. "*" indicates a significant correlation. SSA – specific surface area

hydrogen bonds with H_2O molecules than nitrogen- and oxygen-containing groups, resulting in easier evaporation of H_2O molecules. Hence, the wheat straw biochar produced at 300 ℃ in air-limitation exhibited a high k_e. Wheat straw biochar produced at 300–450 ℃ in N_2-flow exhibited the lowest k_e for all the studied biochars (Fig. 6a), which further confirmed that nitrogen- and oxygen-containing groups were the primary factor to reduce the evaporation of biochar-bound water. In addition, pine sawdust biochar produced in CO_2-flow at 750 ℃ (k_e – 0.0221 ± 0.0033 min^{-1}) exhibited the lowest k_e than the biochars produced at 300 – 600 ℃ (k_e of the other biochars – from 0.0263 ± 0.0020 to 0.0326 ± 0.0030 min^{-1}). It could be seen from Additional file 1: Table S1 that the pine sawdust biochar produced at 750 ℃ in CO_2-flow had about the same elemental composition as the pine sawdust biochars produced at 300 – 600 ℃ in CO_2-flow, but presented a significantly higher SSA (424 $m^2 \cdot g^{-1}$) compared to all the other biochars where micropore area varied from 0.17 to 129 $m^2 \cdot g^{-1}$. Hence, it could be suggested that SSA was the important factor to reduce the evaporation of water bound to pine sawdust biochar produced at 750 ℃ in CO_2-flow (Lataf et al. 2022; Gray et al. 2014).

The correlation analysis was further used to explore the main controlling mechanisms on the evaporation of biochar-bound water (Fig. 6c). The k_e value of biochar-bound water showed significantly positive correlations with the biochar carbon content, pH, C–C or C=C, and significant negative correlations with nitrogen, and oxygen contents, H/C and (O + N)/C ratios, and with C=O group content. Higher content of carbon in C–C or C=C groups (aliphatic and aromatic carbon) represented higher hydrophobicity of biochar surface (Mao et al. 2019; Adhikari et al. 2023) thus increasing the repulsion

between the surface of biochar and H_2O molecules, eventually supporting the evaporation of biochar-bound water. High pH indicates that H_2O molecules are mainly present in the form of OH^- which generates strong electrostatic repulsion with the negatively charged nitrogen- and oxygen-containing groups of biochar resulting in an increased repulsion between the surface of biochar and H_2O molecules and causing enhanced evaporation of biochar-bound water. For the studied biochars, nitrogen was dominated by pyridinic and pyrrolic forms (Additional file 1: Fig. S3), and oxygen was mainly in the forms of C=O and C–O bonds (Additional file 1: Fig. S2). These forms of nitrogen and oxygen have strong negative charges (from –0.84 to –0.51) (Table 1) and unshared electronic pairs. They can serve as receptors of hydrogen bond to link H_2O molecules together (hydrogen of H_2O as the donor of hydrogen bond) (Gilli and Gilli 2014) (Fig. 5). Thus nitrogen and oxygen content, C–O and (O+N)/C values could reduce the evaporation of biochar-bound water. Likewise, higher H/C values represent more aliphatic carbon (e.g., alkylate carbon), and the hydrogen of the aliphatic structure is weakly positively charged. It can be a donor of hydrogen bond to link to the H_2O molecule (oxygen of H_2O as a receptor of hydrogen bond) (Gilli and Gilli 2014) (Fig. 5). Thus, the H/C ratio has a significant negative correlation with the evaporation of biochar-bound water.

As specified above, the correlation analysis can help to explore the relationship between the evaporation of biochar-bound water and some of its controlling parameters such as certain properties of biochar. Still, the quantitative importance of biochar's various properties to the evaporation of biochar-bound water remains unclear. Herein, the hierarchical partitioning was adopted by introducing the hierarchical partitioning method to quantify the importance of biochar's studied properties to the evaporation of biochar-bound water (Lai et al. 2022). The results are shown in Fig. 6d. In this study, oxygen, nitrogen, and carbon contents had approximately the same high importance (from 0.09 to 0.10) for the evaporation of biochar-bound water. The primary reason was that H_2O binding to biochar surface mainly relied on the strong hydrogen bond between oxygen- and nitrogen-containing functional groups and H_2O molecules. Meanwhile, more carbon atoms indicated fewer oxygen- and nitrogen-containing functional groups (carbon content presented a significantly negative correlation with oxygen and nitrogen contents, Additional file 1: Fig. S4). Besides, hydrogen content, ash, and SSA presented a relatively low importance (<0.05) for the evaporation of biochar-bound water, and the correlation was insignificant ($p>0.05$) (Fig. 6c, d). In addition, H/C and pH were significantly correlated with the evaporation of biochar-bound water, but they had lower importance to the evaporation of biochar-bound water. Though higher H/C represented more aliphatic hydrogen (as the hydrogen bond donor) which could also form hydrogen bond with H_2O molecules, the hydrogen bond is very weak (Gilli and Gilli 2014). The H/C ratio thereby played a secondary important role in the evaporation of biochar-bound water. The biochar-bound water molecules (water molecules binding with nitrogen- and oxygen-containing groups) were mainly in the form of H_2O rather than OH^- (Gilli and Gilli 2014) (Fig. 5), thus pH presented a low importance for the evaporation of biochar-bound water. Consequently, increasing oxygen and nitrogen content in biochar is an effective way to reduce the evaporation of biochar-bound water.

4 Conclusions

This study found that nitrogen- and oxygen-containing groups as well as aliphatic hydrogen improved the WHC of the studied biochars and decreased the evaporation of biochar-bound water. Biochar nitrogen was mainly in pyridinic and pyrrolic forms and oxygen was in the form of C=O and C–O; these forms of nitrogen and oxygen could be receptors of hydrogen bonds to link to H_2O molecules. Aliphatic hydrogen could be a donor of hydrogen bond to link to the H_2O molecule. Nitrogen content (importance – 0.31) played a most important role in the WHC of the biochars than the other studied parameters (including carbon, oxygen, hydrogen, ash contents, pH, and SSA importance from 0.02 to 0.09). Furthermore, in all the studied biochar properties, nitrogen, oxygen, and carbon content had the highest importance for the evaporation of biochar-bound water. Consequently, producing biochar rich in nitrogen- and oxygen-containing groups (especially nitrogen-containing groups) and amending them into the soil can be an effective way to maintain soil moisture. In addition, this study mainly focused on exploring the mechanism of the effect that biochar properties have on its WHC and biochar-bound water evaporation by using a laboratory simulation experiment. The future direction of the study could be a field experiment with the application of nitrogen-rich biochar into a real soil environment, elucidating the mechanism for nitrogen-rich biochar-soil interaction affecting the soil WHC and water evaporation.

Supplementary Information

The online version contains supplementary material available at https://doi.org/10.1007/s42773-024-00317-2.

Additional file 1: Table S1. Selected properties of biochars. **Fig. S1.** Fourier transform infrared (FTIR) spectra of different biochars. Biochars: AW – wheat straw biochar produced in air-limitation, CW – wheat straw biochar produced in CO_2-flow, NW – wheat straw biochar produced in

N_2-flow, AP – pine sawdust biochars produced in air-limitation, CP – pine sawdust biochars produced in CO_2-flow, and NP – pine sawdust biochars produced in N_2-flow. The numbers 300, 450, 600, and 750 represent the pyrolytic temperature. **Fig. S2.** C1s peak in X-ray photoelectron spectroscopy (XPS) spectra of biochars and the abundances of surface chemical groups in biochars. Biochars: AW – wheat straw biochar produced in air-limitation, CW – wheat straw biochar produced in CO_2-flow, NW – wheat straw biochar produced in N_2-flow, AP – pine sawdust biochars produced in air-limitation, CP – pine sawdust biochars produced in CO_2-flow, and NP – pine sawdust biochars produced in N_2-flow. The numbers 300, 450, 600, and 750 represent the pyrolytic temperature. **Fig. S3.** N1s peak in X-ray photoelectron spectroscopy (XPS) spectra of biochars and the abundances of surface chemical groups in biochars. Biochars: AW – wheat straw biochar produced in air-limitation, CW – wheat straw biochar produced in CO_2-flow, NW – wheat straw biochar produced in N_2-flow, AP – pine sawdust biochars produced in air-limitation, CP – pine sawdust biochars produced in CO_2-flow, and NP – pine sawdust biochars produced in N_2-flow. The numbers 300, 450, 600, and 750 represent the pyrolytic temperature. **Fig. S4.** Correlation matrix of the properties of biochars. SSA – specific surface area.

Acknowledgements
We are grateful to the National Natural Science Foundation and the Fujian Provincial Natural Science Foundation for funding this research.

Author contributions
All authors contributed to the study concept and design. Investigation was performed by HZ, YC, YZ, JN, and RW; original draft writing—by HZ; validation—by YC and YZ; editing—by JN and RW; conceptualization, supervision, writing, reviewing and editing—by WC.

Funding
This project was supported by the National Natural Science Foundation of China (Grant 42077130), the Natural Science Foundation of Fujian Province, China (Grant 2020J01137, 2022R1002003).

Data availability
The datasets used or analyzed during the current study are available from the corresponding author on reasonable request.

Declarations

Competing interests
The authors declare that they have no competing financial interests or personal relationships that could have appeared to influence the work reported in this paper.

Author details
[1]Key Laboratory for Humid Subtropical Eco-Geographical Processes of the Ministry of Education/Fujian Provincial Key Laboratory for Plant Eco-Physiology/Institute of Geography, School of Geographical Sciences, Fujian Normal University, Fuzhou 350007, Fujian, China.

Received: 8 September 2023 Revised: 1 March 2024 Accepted: 2 March 2024
Published online: 27 March 2024

References

Adhikari S, Timms W, Parvez Mahmud MA (2022) Optimising water holding capacity and hydrophobicity of biochar for soil amendment—a review. Sci Total Environ 851:158043
Adhikari S, Parvez Mahmud MA, Nguyen MD, Timms W (2023) Evaluating fundamental biochar properties in relation to water holding capacity. Chemosphere 2023(328):138620
Basso AS, Miguez FE, Laird DA, Horton R, Westgate M (2013) Assessing potential of biochar for increasing water-holding capacity of sandy soils. GCB Bioenergy 5:132–143
Blanco-Canqui H (2017) Biochar and soil physical properties. Soil Sci Soc Am J 81:687–711
Chen Y, Liu B, Yang H, Yang Q, Chen H (2014) Evolution of functional groups and pore structure during cotton and corn stalks torrefaction and its correlation with hydrophobicity. Fuel 137:41–49
Chen W, Wei R, Yang L, Yang Y, Li G, Ni J (2019) Characteristics of wood-derived biochars produced at different temperatures before and after deashing: Their different potential advantages in environmental applications. Sci Total Environ 651:2762–2771
Chen Y, Syed-Hassan SSA, Xiong Z, Li Q, Hu X, Xu J, Ren Q, Deng Z, Wang X, Su S, Hu S, Wang Y, Xiang J (2021) Temporal and spatial evolution of biochar chemical structure during biomass pellet pyrolysis from the insights of micro-Raman spectroscopy. Fuel Process Technol 218:106839
Gao W, Lin Z, Chen H, Yan S, Huang Y, Hu X, Zhang S (2022) A review on N-doped biochar for enhanced water treatment and emerging applications. Fuel Process Technol 237:107468
Gilli G, Gilli P (2014) The nature of the hydrogen bond: Outline of a comprehensive hydrogen bond theory. Oxford University Press, Oxford
Gray M, Johnson MG, Dragila MI, Kleber M (2014) Water uptake in biochars: the roles of porosity and hydrophobicity. Biomass Bioenerg 61:196–205
Hamidzadeh Z, Ghorbannezhad P, Ketabchi MR, Yeganeh B (2023) Biomass-derived biochar and its application in agriculture. Fuel 341:127701
Hien TTT, Tsubota T, Taniguchi T, Shinogi Y (2021) Enhancing soil water holding capacity and provision of a potassium source via optimization of the pyrolysis of bamboo biochar. Biochar 3:51–61
Ibrahimi K, Alghamdi AG (2022) Available water capacity of sandy soils as affected by biochar application: a meta-analysis. CATENA 214:106281
Jang HM, Kan E (2019) Engineered biochar from agricultural waste for removal of tetracycline in water. Bioresour Technol 284:437–447
Kim P, Johnson A, Edmunds CW, Radosevich M, Vogt F, Rials TG, Labbé N (2011) Surface functionality and carbon structures in lignocellulosic-derived biochars produced by fast pyrolysis. Energy Fuel 25:4693–4703
Lai J, Zou Y, Zhang J, Peres-Neto PR (2022) Generalizing hierarchical and variation partitioning in multiple regression and canonical analyses using the rdacca.hp R package. Methods Ecol Evol 13:782–788
Lataf A, Carleer R, Yperman J, Marchal W, Vandamme D, Jozefczak M, Cuypers A, Vandecasteele B, Viaene J, Schreurs S (2022) The effect of pyrolysis temperature and feedstock on biochar agronomic properties. J Anal Appl Pyrol 168:105728
Lazar P, Mach R, Otyepka M (2019) Spectroscopic fingerprints of graphitic, pyrrolic, pyridinic, and chemisorbed nitrogen in N-doped graphene. J Phys Chem C 123:10695–10702
Leng L, Xiong Q, Yang L, Li H, Zhou Y, Zhang W, Jiang S, Li H, Huang H (2021) An overview on engineering the surface area and porosity of biochar. Sci Total Environ 763:144204
Li H, Tan Z (2021) Preparation of high water-retaining biochar and its mechanism of alleviating drought stress in the soil and plant system. Biochar 3:579–590
Li S, Shao L, Zhang H, He P, Lü F (2020) Quantifying the contributions of surface area and redox-active moieties to electron exchange capacities of biochar. J Hazard Mater 394:122541
Liu Q, Li D, Cheng H, Cheng J, Du K, Hu Y, Chen Y (2021) High mesoporosity phosphorus-containing biochar fabricated from *Camellia oleifera* shells: Impressive tetracycline adsorption performance and promotion of pyrophosphate-like surface functional groups (C-O-P bond). Bioresour Technol 329:124922
Mao J, Zhang K, Chen B (2019) Linking hydrophobicity of biochar to the water repellency and water holding capacity of biochar-amended soil. Environ Poll 253:779–789
Muzyka R, Misztal E, Hrabak J, Banks SW, Sajdak M (2023) Various biomass pyrolysis conditions influence the porosity and pore size distribution of biochar. Energy 263:126128
Nzediegwu C, Arshad M, Ulah A, Naeth MA, Chang SX (2021) Fuel, thermal and surface properties of microwave-pyrolyzed biochars depend on feedstock type and pyrolysis temperature. Bioresour Technol 320:124282
Omondi MO, Xia X, Nahayo A, Liu X, Korai PK, Pan G (2016) Quantification of biochar effects on soil hydrological properties using meta-analysis of literature data. Geoderma 274:28–34

Oppong Danso E, Monnie F, Abenney-Mickson S, Arthur E, Benjamin Sabi E, Neumann Andersen M (2021) Does biochar particle size, application rate and irrigation regime interact to afect soil water holding capacity, maize growth and nutrient uptake? J Soil Sci Plant Nut 21:3180–3193

Seitz S, Teuber S, Geißler C, Goebes P, Scholten T (2020) How do newly-amended biochar particles affect erodibility and soil water movement?-a small-scale experimental approach. Soil Syst 4:60

Singh B, Fang Y, Cowie BCC, Thomsen L (2014) NEXAFS and XPS characterisation of carbon functional groups of fresh and aged biochars. Org Geochem 77:1–10

Suliman W, Harsh JB, Abu-Lail NI, Fortuna AM, Dallmeyer I, Garcia-Perez M (2017) The role of biochar porosity and surface functionality in augmenting hydrologic properties of a sandy soil. Sci Total Environ 574:139–147

Wang D, Zhang W, Hao X, Zhou D (2013) Transport of biochar particles in saturated granular media: effects of pyrolysis temperature and particle size. Environ Sci Technol 47:821–828

Weber K, Quicker P (2018) Properties of biochar. Fuel 217:240–261

Werdin J, Conn R, Fletcher TD, Rayner JP, Williams NSG, Claire Farrell C (2021) Biochar particle size and amendment rate are more important for water retention and weight of green roof substrates than differences in feedstock type. Ecol Eng 171:106391

Wiersma W, van der Ploeg MJ, Sauren IJMH, Stoof CR (2020) No effect of pyrolysis temperature and feedstock type on hydraulic properties of biochar and amended sandy soil. Geoderma 364:114209

Wu L, Ni J, Zhang H, Yu S, Wei R, Qian W, Chen W, Qi Z (2022) The composition, energy, and carbon stability characteristics of biochars derived from thermo-conversion of biomass in air-limitation, CO_2, and N_2 at different temperatures. Waste Manag 141:136–146

Xiang Y, Zhang H, Yu S, Ni J, Wei R, Chen W (2022) Influence of pyrolysis atmosphere and temperature co-regulation on the sorption of tetracycline onto biochar: structure-performance relationship variation. Bioresour Technol 360:127647

Yang C, Liu J, Lu S (2021) Pyrolysis temperature affects pore characteristics of rice straw and canola stalk biochars and biochar-amended soils. Geoderma 397:11097

Yang J, Yang H, Wang S, Wang K, Sun Y, Yi W, Yang G (2023) Importance of pyrolysis programs in enhancing the application of microalgae-derived biochar in microbial fuel cells. Fuel 333:126244

Yu S, Wu L, Ni J, Zhang H, Wei R, Chen W (2022) The chemical compositions and carbon structures of pine sawdust- and wheat straw-derived biochars produced in air-limitation, carbon dioxide, and nitrogen atmospheres, and their variation with charring temperature. Fuel 315:122852

Zhang J, Chen Q, You C (2016) Biochar effect on water evaporation and hydraulic conductivity in sandy soil. Pedosphere 26:265–272

Zhang H, Chen W, Li Q, Zhang X, Wang C, Yang L, Wei R, Ni J (2020) Difference in characteristics and nutrient retention between biochars produced in nitrogen-flow and air-limitation atmospheres. J Environ Qual 49:1396–1407

Zhang J, Amonette JE, Flury M (2021) Effect of biochar and biochar particle size on plant available water of sand, silt loam, and clay soil. Soil till Res 212:104992

Zhao L, Cao X, Masek O, Zimmerman A (2013) Heterogeneity of biochar properties as a function of feedstock sources and production temperatures. J Hazard Mater 256–257:1–9

Zornoza R, Moreno-Barriga F, Acosta JA, Munoz MA, Faz A (2016) Stability, nutrient availability and hydrophobicity of biochars derived from manure, crop residues, and municipal solid waste for their use as soil amendments. Chemosphere 144:122–130